J. Fluid Mech. (2014), *vol.* 741, *pp* 658–680.
doi:10.1017/jfm.2014.5

Non-Boussinesq gravity currents propagating on different bottom slopes

Albert Dai†

Department of Water Resources and Environmental Engineering, Tamkang University, Taiwan

(Received 1 August 2013; revised 10 December 2013; accepted 23 December 2013)

Experiments on the non-Boussinesq gravity currents generated from an instantaneous buoyancy source propagating on an inclined boundary in the slope angle range $0^\circ \leqslant \theta \leqslant 9^\circ$ with relative density difference in the range of $0.05 \leqslant \epsilon \leqslant 0.17$ are reported, where $\epsilon = (\rho_1 - \rho_0)/\rho_0$, with ρ_1 and ρ_0 the densities of the heavy and light ambient fluids, respectively. We showed that a 3/2 power-law, $(x_f + x_0)^{3/2} = K_M^{3/2} {B_0'}^{1/2}(t + t_{I0})$, exists between the front location measured from the virtual origin, $(x_f + x_0)$, and time, t, in the early deceleration phase for both the Boussinesq and non-Boussinesq cases, where K_M is a measured empirical constant, B_0' is the total released buoyancy, and t_{I0} is the t-intercept. Our results show that K_M not only increases as the relative density difference increases but also assumes its maximum value at $\theta \approx 6^\circ$ for sufficiently large relative density differences. In the late deceleration phase, the front location data deviate from the 3/2 power-law and the flow patterns on $\theta = 6^\circ, 9^\circ$ slopes are qualitatively different from those on $\theta = 0^\circ, 2^\circ$. In the late deceleration phase, we showed that viscous effects could become more important and another power-law, $(x_f + x_0)^2 = K_V^2 {B_0'}^{2/3} A_0^{1/3} \nu^{-1/3}(t + t_{V0})$, applies for both the Boussinesq and non-Boussinesq cases, where K_V is an empirical constant, A_0 is the initial volume of heavy fluid per unit width, ν is the kinematic viscosity of the fluids, and t_{V0} is the t-intercept. Our results also show that K_V increases as the relative density difference increases and K_V assumes its maximum value at $\theta \approx 6^\circ$.

Key words: geophysical and geological flows, gravity currents

1. Introduction

Gravity currents, also known as density currents, are flows driven by a density difference. A number of factors that are likely to cause variations in the density of fluid include temperature differentials, dissolved materials, and suspended sediments. A large number of laboratory studies have been performed for such flows in a closed horizontal channel with a vertical barrier, where each side of the barrier is filled with fluid of different density. Removal of the barrier then sets the two fluids into motion. This type of experiment, i.e. lock-exchange flow, serves as a model for a variety of geophysical and industrial flows (Allen 1985; Simpson 1997). Lock-exchange flows have received much attention in the literature and most of these

† Email address for correspondence: hdai@mail.tku.edu.tw

experiments were for the Boussinesq case, i.e. the densities of the two fluids were only slightly different, e.g. (e.g. Shin, Dalziel & Linden 2004; Marino, Thomas & Linden 2005; Cantero *et al.* 2007; La Rocca *et al.* 2008, 2012*a*,*b*; Adduce, Sciortino & Proietti 2012). Although the Boussinesq case is representative of most geophysical flows, the non-Boussinesq case, where the density difference is significantly larger, is important in quite a few situations. Fires in a tunnel produce gravity currents with hot combustion products, the density of which is significantly less than air due to high temperatures. In powder-snow avalanches, the excess density due to the suspended snow grains is large compared with that of air. Pyroclastic flows from volcanic eruptions often take the form of gravity currents and the density within the flow due to hot ash and rocks is also significantly larger than the surrounding air. Sediment-laden rivers form turbidity underflows in a lake or reservoir, and it is not uncommon to observe high sediment concentrations due to extreme precipitation events in the watershed. Among others, laboratory studies on the non-Boussinesq lock-exchange flows were reported by Keller & Chyou (1991), Grobelbauer, Fannelop & Britter (1993), Lowe, Rottman & Linden (2005), and two-dimensional numerical simulations were performed by Birman, Martin & Meiburg (2005).

Gravity currents propagating down an inclined boundary have been considered less often, but are also commonly encountered in geophysical environments and engineering applications, such as powder-snow avalanches (Hopfinger 1983) and spillage of hazardous materials (Fannelop 1994). Gravity currents down an inclined boundary can be produced with a continuous, negatively buoyant inflow (Britter & Linden 1980; Baines 2001, 2005; Cenedese & Adduce 2008) or can be a surge-type flow generated from the release of a finite volume of buoyancy (Beghin, Hopfinger & Britter 1981; Monaghan *et al.* 1999; Dai & Garcia 2010). For gravity currents produced from an instantaneous source on a slope, it is known that after the heavy fluid is released, the gravity currents first go through an acceleration phase followed by a deceleration phase. To describe the front velocity history for gravity currents from an instantaneous source on a slope, Beghin *et al.* (1981) developed the thermal theory for the Boussinesq case which has formed the basis for subsequent studies, (e.g. Dade, Lister & Huppert 1994; Rastello & Hopfinger 2004). Among other studies related to the present work, Birman *et al.* (2007) reported two-dimensional simulations of the full-depth lock-exchange problem on a slope and Seon *et al.* (2007) performed lock-exchange experiments in tilted tubes, but the geometric configurations therein make the thermal theory less applicable in their problems. We should point out that none of the above work is for the non-Boussinesq case.

More recently, also looking at the Boussinesq gravity currents from an instantaneous source on a slope, Maxworthy & Nokes (2007) reported that the released heavy fluid continuously feeds the gravity current head with buoyancy in the acceleration phase from the following tail current, like a line plume, and such flow patterns occur in particular when the lock length is significantly greater than the lock height. Later, Maxworthy (2010) reported that the gravity current head may lose buoyancy-containing fluid in the deceleration phase; nevertheless, in the whole range of the deceleration phase the front location history robustly follows a $3/2$ power-law, which is essentially an asymptotic form of the solution from thermal theory.

This study is a continuation of the investigation done by Dai (2013), in which the Boussinesq gravity currents from an instantaneous source on a slope were reported, where the initial density difference between the heavy and light fluids was maintained at a constant value lower than the density differences used in the present paper. Our focus here is also on gravity currents produced from a finite volume of heavy fluid

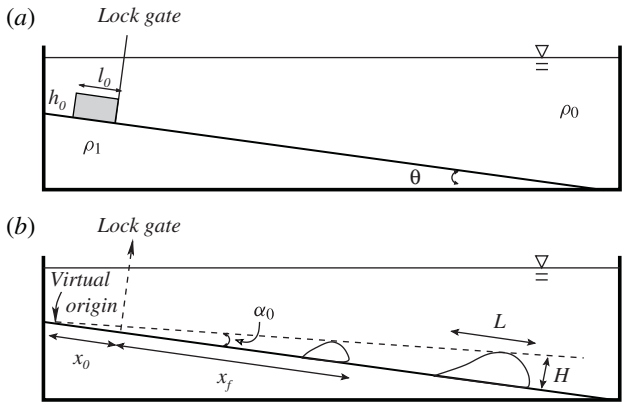

FIGURE 1. Side views of the channel used in the experiments for gravity currents produced from an instantaneous buoyancy source propagating on a slope. The slope angle is θ, the ambient is filled with fluid of density ρ_0, and heavy fluid of density ρ_1 is confined in the lock region. H and L are the height and length of the gravity current head; x_0 is the distance from the virtual origin to the lock gate; x_f is the distance from the gate to the gravity current front. In the initial state, the cross-sectional area of heavy fluid is $A_0 = h_0 l_0$, where $h_0 = 8$ cm and $l_0 = 10$ cm are the lock height and length, respectively. Removal of the gate sets the quiescent heavy fluid into motion.

down an inclined boundary, i.e. the problem set forth in Beghin *et al.* (1981), but with larger relative density differences. The objective is to observe the flow patterns for gravity currents down different bottom slopes and to identify how these patterns change with slope angle. Using the experimental data, quantitative measures for the relationship between the front location and time in the deceleration phase may be derived and the influence of relative density difference is clearly shown for the first time. In § 2, we summarize the power-laws for the front location history in the early and late stages of the deceleration phase. The apparatus and experimental techniques are described in § 3. The qualitative and quantitative results are presented in § 4. Finally, conclusions are drawn in § 5.

2. Theoretical background

The configuration of the problem is sketched in figure 1. Here the nomenclature mainly follows Beghin *et al.* (1981) for the reader's convenience. The density of ambient fluid is taken as ρ_0 and the density of heavy fluid in the lock region is ρ_1, where the relative density difference is $\epsilon = (\rho_1 - \rho_0)/\rho_0$. For non-Boussinesq gravity currents, a commonly used parameter characterizing the density difference is the density ratio, $\gamma = \rho_0/\rho_1$, i.e. $\gamma = 1/(1 + \epsilon)$. The cross-sectional area of the lock, which represents the amount of heavy fluid in the lock, is A_0. After an instantaneous removal of the lock gate, the gravity current head develops and the head approximately takes a semi-elliptical shape with a height-to-length aspect ratio $k = H/L$.

The convection of the gravity current is driven by the heavy fluid contained within the head. Therefore, the linear momentum equation takes the form

$$\frac{\mathrm{d}(\rho + k_v \rho_0) S_1 HLU}{\mathrm{d}t} = B \sin\theta, \tag{2.1}$$

where ρ is the density of mixed fluid in the head, U is the mass-centre velocity of the head, t is the time, $k_v = 2k$ is the added mass coefficient (Batchelor 1967), $S_1 = \pi/4$ is a shape factor by which the cross-sectional area of the semi-elliptical head is defined as S_1HL, and $B = g(\rho - \rho_0)S_1HL$ denotes the buoyancy in the head, where g is acceleration due to gravity. Friction on the slope has been considered minor and can be neglected for slope angles greater than a few degrees (Beghin *et al.* 1981; Ross, Dalziel & Linden 2006). We may assume that the actual amount of heavy fluid in the head is represented by χA_0, i.e. only a fraction χ of heavy fluid in the lock is contained in the head, and the buoyancy is

$$B = \chi g(\rho_1 - \rho_0)A_0, \tag{2.2}$$

where Beghin *et al.* (1981) assumed that $\chi = 1$ and Maxworthy (2010), Dai (2013) experimentally found that $\chi < 1$. Typically the parameter χ should be determined by experiments and cannot be evaluated based on theoretical arguments. As such, χ is unspecified at this point in our framework. With turbulent entrainment assumptions (Ellison & Turner 1959), the mass conservation takes the form

$$\frac{\mathrm{d}}{\mathrm{d}t}(S_1HL) = S_2(HL)^{1/2}\alpha U, \tag{2.3}$$

where $S_2 = (\pi/2^{3/2})(4k^2+1)^{1/2}/k^{1/2}$ is another shape factor by which the circumference of the semi-elliptical head is defined as $S_2(HL)^{1/2}$ and α is the entrainment coefficient.

From (2.3)

$$H = \frac{1}{2}\frac{S_2}{S_1}k^{1/2}\alpha x \quad \text{and} \quad L = \frac{1}{2}\frac{S_2}{S_1}k^{-1/2}\alpha x, \tag{2.4}$$

where x is the distance from the 'virtual origin' to the mass-centre of the gravity current head. Note here that the mass conservation equation (2.3) and its solution (2.4) follow Beghin *et al.* (1981). The 'virtual origin' is located a distance x_0 beyond the lock gate and is found by extrapolating the head height, H, in the upslope direction, as shown in figure 1. The entrainment coefficient α is related to the angle of growth α_0 via the relationship $\alpha = \left(2S_1/S_2k^{1/2}\right)\alpha_0$. Upon substitution of (2.4) into (2.1) and using $U = \mathrm{d}x/\mathrm{d}t$, the momentum equation becomes

$$U\frac{\mathrm{d}}{\mathrm{d}x}(x^2U) + \epsilon\left(\chi\frac{2}{\pi}\frac{k}{1+2k}\frac{A_0}{\alpha_0^2}\right)\frac{\mathrm{d}U^2}{\mathrm{d}x} = C, \tag{2.5}$$

where

$$C = \frac{4}{\pi}\frac{k}{1+2k}\frac{1}{\alpha_0{}^2}\chi B_0'\sin\theta \quad \text{with } B_0' = \epsilon g A_0, \tag{2.6}$$

is the driving force term.

In previous works on the Boussinesq case, e.g. Beghin *et al.* (1981), the influence of density variation on the inertia term, the $O(\epsilon)$ term on the left-hand side of (2.5), has been neglected. For the non-Boussinesq case here, the $O(\epsilon)$ term on the left-hand side of (2.5) is retained and the following closed-form solution is derived:

$$\begin{aligned} U^2 \;=\; & U_0^2\left(\tfrac{1}{2}x_0{}^2 + \epsilon Q\right)^2\left(\tfrac{1}{2}x^2 + \epsilon Q\right)^{-2} \\ & + C\left(\tfrac{1}{6}\left(x^3 - x_0{}^3\right) - \epsilon Q(x - x_0)\right)\left(\tfrac{1}{2}x^2 + \epsilon Q\right)^{-2}, \end{aligned} \tag{2.7}$$

where U_0 is the initial mass-centre velocity and $Q = 2\chi kA_0/(1+2k)\pi\alpha_0^2$.

When the buoyancy source is released with a quiescent initial condition, the solution approaches the following asymptote:

$$U = \left(\tfrac{2}{3}\right)^{1/2} C^{1/2} x^{-1/2}, \tag{2.8}$$

when $x/x_0 \gg 1$ and $x^2/x_0^2 \gg 6\epsilon Q/x_0^2$. Note that the same asymptote is approached for the Boussinesq case when $x/x_0 \gg 1$. Here in the non-Boussinesq case, an additional condition is required, i.e. $x^2/x_0^2 \gg 6\epsilon Q/x_0^2$. It should be pointed out that since $x_0\alpha_0 \approx O(h_0)$, $6\epsilon Q/x_0^2 \approx O(\epsilon)$ and the second condition is no more stringent than the first condition $x/x_0 \gg 1$ as long as $\epsilon \lesssim O(1)$. In other words, it is anticipated that the velocity of non-Boussinesq gravity currents follows the same asymptote in the deceleration phase as the Boussinesq case. As entrainment of ambient fluid reduces the density difference between the fluid in the head and ambient fluid, it is not surprising that non-Boussinesq gravity currents approach the same asymptote as the Boussinesq case for late stages due to the reduced non-Boussinesq effects. In essence, the additional condition for the non-Boussinesq gravity currents to approach the asymptote (2.8), i.e. $x^2/x_0^2 \gg O(\epsilon)$, is equivalent to the statement that the average excess density in the head is small compared with that of ambient fluid. For strong non-Boussinesq effects such that $x^2/x_0^2 \lesssim O(\epsilon)$, the non-Boussinesq gravity currents may not follow (2.8) and the similarity between the non-Boussinesq and Boussinesq cases may not exist. We should keep in mind that entrainment of ambient fluid and, consequently, the angle of growth of the head are important parameters in the thermal theory framework, which then may not be readily applicable to the extreme cases, $\epsilon \gg 1$, such as water and air, because mixing between the two fluids in the extreme cases is very limited.

Since the front location of a gravity current is a relatively easily measurable quantity, it is desirable to rewrite the solution in terms of the front location, x_f, which is measured from the lock gate. Using the geometric relation $(x_f + x_0) = x + L/2$, i.e. $(x_f + x_0) = (1 + \alpha_0/2k)x$, and its time derivative, $u_f = (1 + \alpha_0/2k)U$, the front velocity in the deceleration phase approaches the following asymptote:

$$u_f = \left(\frac{2}{3}\right)^{1/2} C^{1/2} \left(1 + \frac{\alpha_0}{2k}\right)^{3/2} (x_f + x_0)^{-1/2}. \tag{2.9}$$

Upon integration, (2.9) can be rewritten in the following form with an integration constant t_{I0}:

$$(x_f + x_0)^{3/2} = K_M^{3/2} {B_0'}^{1/2} (t + t_{I0}), \tag{2.10}$$

where $K_M = K_B \chi^{1/3}$ and B_0' is the total released buoyancy. The expression for K_B should follow the form

$$K_B = \left(\frac{6}{\pi}\right)^{1/3} \left(1 + \frac{\alpha_0}{2k}\right) \left(\frac{k \sin\theta}{(1 + 2k)\alpha_0^2}\right)^{1/3}. \tag{2.11}$$

After taking the time derivative of (2.10), the front velocity in the deceleration phase follows

$$\frac{u_f (x_f + x_0)^{1/2}}{{B_0'}^{1/2}} = \frac{2}{3} {K_M}^{3/2}, \tag{2.12}$$

which was also the asymptotic form suggested by Beghin *et al.* (1981), who reported for the Boussinesq case that K_M varies approximately between 2.35 and 2.60 at

$\theta = 15^\circ$ and reduces uniformly with increasing θ to a value between 1.56 and 1.87 at $\theta \approx 90^\circ$.

As the gravity force per unit volume of the gravity current head scales as $\rho B_0'(x_f + x_0)^{-2}$ and the inertia scales as $\rho(x_f + x_0)t^{-2}$, the power-law (2.10) is in essence a statement of balance between gravity and inertia forces in the early deceleration phase and $K_M^{3/2}$ is a proportionality constant. In the late deceleration phase when viscous effects become more important, the viscous force per unit volume scales as $\rho\nu(x_f + x_0)t^{-1}\delta^{-1}{A_0}^{-1/2}$, where the viscous stress is estimated as $\rho\nu(x_f + x_0)t^{-1}\delta^{-1}$, and $\delta \sim (\nu t)^{1/2}$ and ${A_0}^{1/2}$ are estimates for the thickness of the boundary layer at the edge of, and an inherent length scale for, the 'active' moving head, respectively (Dai 2013). The balance between gravity and viscous forces then results in

$$(x_f + x_0)^2 = K_V^2 \left(\frac{{B_0'}^2 A_0}{\nu} \right)^{1/3} (t + t_{V0}), \tag{2.13}$$

where K_V^2 is a proportionality constant which has to be determined by experiments and t_{V0} is the t-intercept.

For gravity currents on a horizontal boundary, i.e. lock-exchange flows, the head height does not increase or even slowly decreases as the gravity current propagates; the 'virtual origin' is then taken at the gate (cf. Beghin *et al.* 1981) and (2.12) is equivalent to

$$\tilde{x}_f = K_M \tilde{t}^{2/3} \quad \text{or} \quad \tilde{x}_f^{3/2} = K_M^{3/2} \tilde{t}, \tag{2.14}$$

which is just the asymptotic behaviour for the front location in the inertial phase, where $\tilde{x}_f = x_f/l_0$, $\tilde{t} = t\sqrt{g_0' h_0}/l_0$, and l_0 and h_0 are the lock length and lock height, respectively. Among other values, $K_M = 1.6$ and 1.47 were proposed by Hoult (1972) and Huppert & Simpson (1980), respectively, whereas more recently Marino *et al.* (2005) suggested that K_M varies between 1.3 and 1.6 for full-depth releases and between 1.4 and 1.8 for partial-depth releases. However, recall that all of the above reports are for the Boussinesq case. It is well known that following the inertial phase is the viscous phase, in which the front velocity decays more rapidly than in the inertial phase. For example, Hoult (1972) derived $\tilde{x}_f \sim \tilde{t}^{3/8}$ by considering a balance between the viscous force from the interface and the buoyancy and Huppert (1982) revised the analysis by adding the viscous effects over a rigid horizontal surface and reported that $\tilde{x}_f \sim \tilde{t}^{1/5}$.

3. Experiments

The channel used in the experiments was manufactured with a rectangular cross-section 0.2 m wide, 0.60 m deep and 2.5 m long with transparent Perspex sidewalls. A Perspex board, which is 2.47 m long and slightly less than 0.2 m wide, was placed in the channel as the inclined slope, the angle of which can be adjusted in the range of $0^\circ \leqslant \theta \leqslant 9^\circ$. The channel was reinforced by a specially designed steel cage. A sketch of the experimental set-up was shown in figure 1. The edges of the board were sealed with rubber sponge to prevent leakage of fluid through the slits between the board and the sidewalls of the channel. During the experiments, the less dense fluid was fresh water and filled the channel outside of the lock region. A solution of sodium chloride was injected into the lock as the heavy fluid and the lock was mounted on the higher end of the inclined slope. The lock height and lock length are 8 cm and 10 cm, respectively, and removing the lock gate sets the heavy fluid into motion.

An electric light sheet and a light-diffusing screen were placed against the back wall. A Jai CVM 4+CL CCD camera (1390 × 1024 pixel resolution at 24 frames per second) was positioned 6 m away from, and normal to, the front wall. The camera was rotated with the inclined board such that the x and y axes in the images align with the downslope and wall-normal directions. The heavy fluid in the lock was dyed with a trace of potassium permanganate to provide flow visualization. The dye absorbed the light along the path from the back to the front wall of the channel, and the light intensity was measured and calibrated to give width-averaged concentration via the software DigiFlow (Dalziel 2012). Since potassium permanganate diffuses at about the same rate as sodium chloride, the dye concentration, c, can be used as a surrogate for the sodium chloride concentration and, therefore, the fluid density may be inferred (Shin *et al.* 2004; Marino *et al.* 2005; Nogueira *et al.* 2013*a*,*b*), i.e. $\rho = \rho_0 + c(\rho_1 - \rho_0)$. Images of the gravity current were recorded directly onto a PC with a time resolution of 0.5 s using the same software.

Densities of the fresh water and heavy fluid injected into the lock were measured using a density meter with an accuracy of 10^{-4} g cm^{-3}. The reduced gravity is $g'_0 = g(\rho_1 - \rho_0)/\rho_0$, where ρ_0 and ρ_1 are the densities of the light and heavy fluids, respectively. The kinematic viscosity of the sodium chloride solution is taken as $\nu = 1.1 \times 10^{-2}$ cm^2 s^{-1}. While $\rho_0 \approx 0.9979$ g cm^{-3} was maintained fixed in the experiments, three different ρ_1 values were chosen, i.e. $\rho_1 \approx 1.0478$, 1.0978 and 1.1678 g cm^{-3}. Therefore, the reduced gravity here approximately ranges from 49.05 to 167.02 cm s^{-2}. Density differences in the experiments were chosen such that the produced gravity currents had Reynolds numbers in excess of 1000, above which viscous effects have been thought to be unimportant (Simpson 1997). In all experiments, the lock was submerged beneath the water surface by at least 10 cm to reduce the influence from the free surface. From viewing the gravity current images, it is somewhat difficult to determine the rearward boundary of the head, since shedding of mixed fluid in the form of large, dyed vortices took place and the demarcation was hard to see. It is thus necessary to view the video in real time and make a subjective judgement of the length of the gravity current head, L.

With the width-averaged concentration and the length of the head, the amount of heavy fluid in the head region can be calculated according to

$$\frac{A_h}{A_0} = \frac{1}{A_0} \int_{x_f - L}^{x_f} \int_0^{\infty} c(x, y)\, \mathrm{d}y\, \mathrm{d}x, \tag{3.1}$$

where A_h/A_0 represents the ratio of the amount of heavy fluid in the head region to the total released heavy fluid, x and y are the coordinates in the streamwise and wall-normal directions, respectively. The length of the head, L, in (3.1) is a variable distance between the front location and the end of the head, where the end of the head has to be determined by viewing the video, as done in previous studies, and discussed above.

4. Results

In what follows the experimental results for gravity currents produced from a buoyancy source of $h_0/l_0 = 8$ cm/10 cm on slopes $\theta = 9°$, 6°, 2° and 0° are presented in turn. On each slope, three different density ratios were chosen, i.e. $\gamma = \rho_0/\rho_1 \approx 0.95$, 0.91 and 0.85, or equivalently in terms of the relative density differences, i.e. $\epsilon = (\rho_1 - \rho_0)/\rho_0 \approx 0.05$, 0.10 and 0.17. Other operational parameters and dependent variables are listed in tables 1 and 2. At least five experiments were

Case	θ (deg.)	γ; ϵ	g_0' (cm s^{-2})	t_{max} (s)	$x_{f\,max}$ (cm)	$u_{f\,max}$ (cm s^{-1})	$A_{h,max}/A_0$
9I	9	≈ 0.85; ≈ 0.17	$166.97^{+0.07}_{-0.03}$	$3.7^{+0.3}_{-0.2}$	$76.08^{+11.20}_{-5.92}$	$25.28^{+0.27}_{-0.27}$	$0.63^{+0.03}_{-0.02}$
9II	9	≈ 0.91; ≈ 0.10	$97.99^{+0.31}_{-0.26}$	$4.3^{+0.2}_{-0.3}$	$71.42^{+4.96}_{-5.32}$	$19.10^{+0.21}_{-0.22}$	$0.57^{+0.05}_{-0.09}$
9III	9	≈ 0.95; ≈ 0.05	$49.15^{+0.01}_{-0.01}$	$5.7^{+0.8}_{-1.7}$	$65.40^{+9.69}_{-17.38}$	$13.10^{+0.28}_{-0.27}$	$0.68^{+0.01}_{-0.01}$
6I	6	≈ 0.85; ≈ 0.17	$166.81^{+0.09}_{-0.09}$	$3.7^{+0.3}_{-0.2}$	$71.18^{+8.76}_{-7.54}$	$23.44^{+0.21}_{-0.16}$	$0.56^{+0.04}_{-0.07}$
6II	6	≈ 0.91; ≈ 0.10	$98.14^{+0.35}_{-0.22}$	$4.0^{+0.5}_{-1.0}$	$64.68^{+5.38}_{-10.15}$	$18.36^{+0.19}_{-0.26}$	$0.59^{+0.04}_{-0.07}$
6III	6	≈ 0.95; ≈ 0.05	$49.09^{+0.06}_{-0.13}$	$5.3^{+0.7}_{-0.8}$	$59.02^{+9.66}_{-12.69}$	$13.14^{+0.41}_{-0.27}$	$0.67^{+0.02}_{-0.03}$
2I	2	≈ 0.85; ≈ 0.17	$167.01^{+0.01}_{-0.01}$	$2.5^{+0.0}_{-0.0}$	$44.84^{+5.42}_{-4.58}$	$21.38^{+0.26}_{-0.31}$	$0.54^{+0.04}_{-0.04}$
2II	2	≈ 0.91; ≈ 0.10	$98.02^{+0.37}_{-0.28}$	$2.8^{+1.2}_{-0.8}$	$39.33^{+14.63}_{-10.14}$	$16.36^{+0.16}_{-0.14}$	$0.52^{+0.03}_{-0.03}$
2III	2	≈ 0.95; ≈ 0.05	$49.05^{+0.10}_{-0.10}$	$4.2^{+0.3}_{-0.2}$	$41.65^{+3.96}_{-2.89}$	$11.49^{+0.19}_{-0.17}$	$0.54^{+0.03}_{-0.02}$
0I	0	≈ 0.85; ≈ 0.17	$167.41^{+0.14}_{-0.07}$	$2.5^{+0.0}_{-0.0}$	$40.99^{+1.32}_{-0.78}$	$19.76^{+0.18}_{-0.20}$	—
0II	0	≈ 0.91; ≈ 0.10	$98.75^{+0.17}_{-0.33}$	$3.8^{+1.7}_{-0.3}$	$49.56^{+5.65}_{-8.81}$	$15.16^{+0.43}_{-0.29}$	—
0III	0	≈ 0.95; ≈ 0.05	$49.35^{+0.10}_{-0.10}$	$4.7^{+0.3}_{-1.7}$	$44.51^{+3.87}_{-2.18}$	$11.17^{+0.24}_{-0.25}$	—

TABLE 1. Table showing operational parameters, including the slope angle θ, density ratio γ, relative density difference $\epsilon = (1 - \gamma)/\gamma$, reduced gravity $g_0' = \epsilon g$, the time, t_{max}, and front location, $x_{f\,max}$, at which the gravity current reaches its maximum front velocity, $u_{f\,max}$. The maximum values of the ratio of the buoyancy in the head to the total released buoyancy are listed in $A_{h,max}/A_0$. Each value is the average of five experiments. The lock geometry, i.e. $h_0/l_0 = 8$ cm/10 cm, is maintained fixed for all experiments. The error estimates are to add and subtract the maximum and minimum values and are not the r.m.s. estimates.

Case	k	α_0	$x_0/{A_0}^{1/2}$	$t_{I0}{g_0'}^{1/2}/{A_0}^{1/4}$	$t_{V0}{g_0'}^{1/2}/{A_0}^{1/4}$
9I	$0.23^{+0.02}_{-0.03}$	$0.0183^{+0.0013}_{-0.0007}$	$37.26^{+1.03}_{-1.55}$	$31.83^{+0.93}_{-1.71}$	$21.09^{+2.22}_{-1.90}$
9II	$0.25^{+0.03}_{-0.02}$	$0.0231^{+0.0024}_{-0.0014}$	$30.15^{+0.82}_{-0.51}$	$25.31^{+0.35}_{-0.43}$	$16.56^{+1.84}_{-3.22}$
9III	$0.26^{+0.04}_{-0.04}$	$0.0264^{+0.0008}_{-0.0008}$	$22.53^{+1.09}_{-0.76}$	$18.59^{+1.24}_{-1.04}$	$7.90^{+0.57}_{-0.50}$
6I	$0.27^{+0.03}_{-0.02}$	$0.0097^{+0.0002}_{-0.0002}$	$69.99^{+2.34}_{-1.86}$	$71.41^{+1.97}_{-2.68}$	$56.79^{+4.13}_{-4.78}$
6II	$0.24^{+0.05}_{-0.04}$	$0.0176^{+0.0009}_{-0.0005}$	$38.82^{+1.00}_{-0.72}$	$36.80^{+0.83}_{-0.60}$	$22.31^{+3.68}_{-2.45}$
6III	$0.24^{+0.03}_{-0.04}$	$0.0213^{+0.0004}_{-0.0005}$	$31.39^{+1.41}_{-0.76}$	$28.03^{+1.46}_{-1.32}$	$16.71^{+0.81}_{-0.72}$
2I	$0.26^{+0.02}_{-0.02}$	$0.0057^{+0.0008}_{-0.0008}$	$100.96^{+1.23}_{-1.45}$	$129.81^{+2.92}_{-1.94}$	$128.75^{+3.41}_{-5.43}$
2II	$0.25^{+0.04}_{-0.06}$	$0.0110^{+0.0011}_{-0.0012}$	$53.25^{+2.40}_{-2.87}$	$67.06^{+3.95}_{-5.00}$	$60.00^{+4.60}_{-5.59}$
2III	$0.22^{+0.04}_{-0.04}$	$0.0130^{+0.0003}_{-0.0003}$	$45.79^{+0.81}_{-1.29}$	$57.52^{+3.65}_{-3.89}$	$53.80^{+2.00}_{-3.98}$

TABLE 2. Table showing dependent variables. Each value is the average of five experiments. The lock geometry, i.e. $h_0/l_0 = 8$ cm/10 cm, is maintained fixed for all experiments. The error estimates are to add and subtract the maximum and minimum values and are not the r.m.s. estimates.

performed in each case to make qualitative and quantitative observations. The height and length of the lock, i.e. h_0 and l_0, remained fixed for all reported experiments. Reynolds numbers in the experiments, i.e. $Re = \sqrt{\epsilon g h_0} h_0/\nu$, range from $Re \approx 14\,000$ for $\epsilon \approx 0.05$ ($\gamma \approx 0.95$) to $Re \approx 26\,000$ for $\epsilon \approx 0.17$ ($\gamma \approx 0.85$).

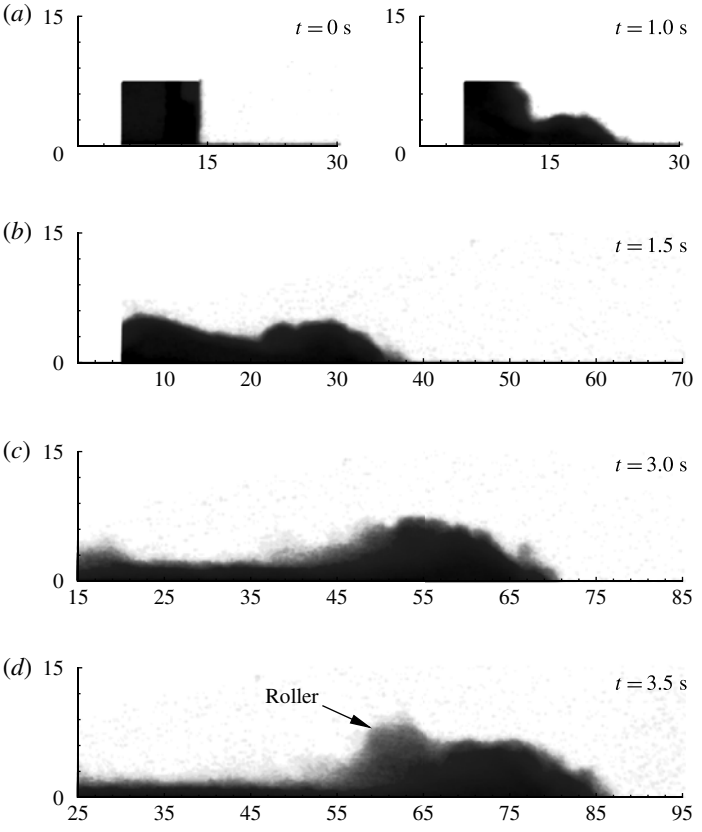

FIGURE 2. Experiment 01/29/13-5: fluid concentration images for the gravity current from a buoyancy source of $h_0/l_0 = 8$ cm/10 cm and $g_0' = 167.10$ cm s^{-2} propagating on a 9° slope. Distances in the downslope and wall-normal directions are in units of centimetres. Time instants are chosen at $t = 0$, 1.0, 1.5, 3.0 and 3.5 s in the acceleration phase. In this case the maximum front velocity $u_f \approx 25.28$ cm s^{-1} and occurs at $t \approx 3.5$ s.

4.1. *Gravity currents on $\theta = 9°$ slope*

4.1.1. *Qualitative features*

The heavy fluid was set into motion when the lock gate was withdrawn. The gravity current produced went from a quiescent initial condition, through an acceleration phase followed by a deceleration phase. Figure 2 presents fluid concentration images for the gravity current with $\epsilon \approx 0.17$ on a 9° slope in the acceleration phase. The initial heavy fluid in the lock of dimensions $h_0/l_0 = 8$ cm/10 cm collapsed with a small head forming at $t = 1.0$ s. As time progressed, the heavy fluid in the lock region was injected into the head, as shown in figure 2 at $t = 1.5$ and 3.0 s. As the gravity current propagated further in the acceleration phase, the head approximately took a semi-elliptical shape with a roller consistently forming behind the head, as shown in figure 2 at $t = 3.5$ s.

Table 1 lists the operational parameters along with the time and front location at which the gravity currents reached their maximum front velocity. We note the fact that given the same slope angle, as the relative density difference increases from $\epsilon \approx 0.05$ to 0.17, the maximum front velocity increases as expected, while the time

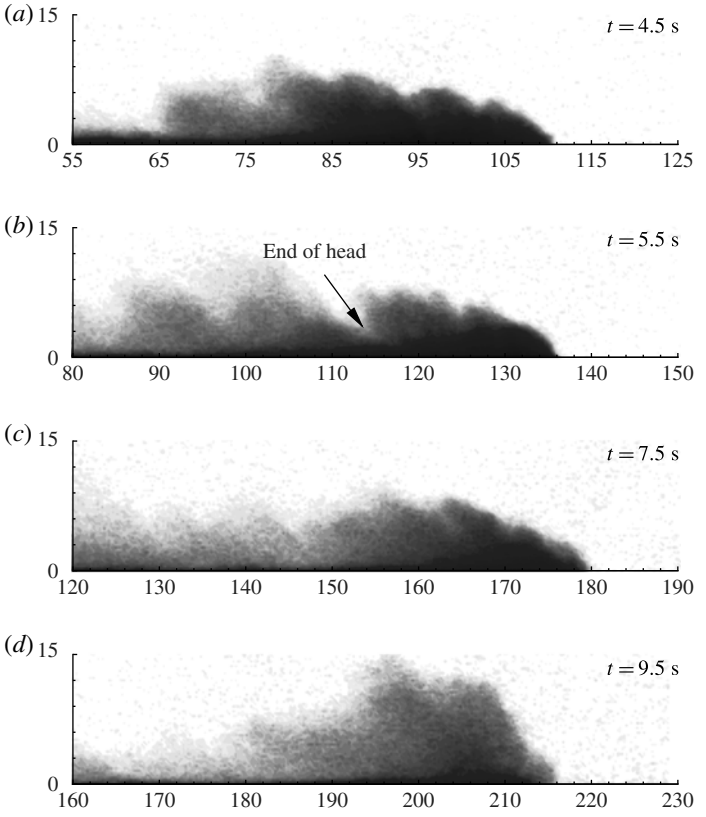

FIGURE 3. Experiment 01/29/13-5: fluid concentration images for the gravity current on a 9° slope. Distances in the downslope and wall-normal directions are in units of centimetres. Time instants are chosen at $t = 4.5$, 5.5, 7.5 and 9.5 s in the deceleration phase.

required for the acceleration phase decreases and the distance for the acceleration phase increases.

Figure 3 presents concentration images for the gravity current with $\epsilon \approx 0.17$ on a 9° slope in the deceleration phase. At this stage of motion, the head maintained a semi-elliptical shape with Kelvin–Helmholtz instabilities between the moving heavy fluid and light ambient fluid. In the deceleration phase, mixed fluid was consistently left behind in the wake region, as shown in figure 3 at $t = 4.5$, 5.5 and 7.5 s. A new flow pattern is identified here for the gravity current with $\epsilon \approx 0.17$ on a 9° slope, as shown in figure 3 at $t = 9.5$ s. The interface between the moving heavy fluid and light ambient fluid, namely the edge of the gravity current head, undergoes a large-scale rolling-up with ambient fluid towards the end of run in the deceleration phase. In fact, this new flow pattern was observed to occur for all the relative density differences considered in this study, i.e. $\epsilon \approx 0.05$, 0.10 and 0.17, for the gravity currents on a 9° slope. Since the qualitative observations for gravity currents with $\epsilon \approx 0.05$ and 0.10 on $\theta = 9°$ are similar to those with $\epsilon \approx 0.17$ as reported, other concentration images for $\epsilon \approx 0.05$ and 0.10 are omitted for brevity, and only the relationships between $(x_f + x_0)^{3/2}$ and t and between $(x_f + x_0)^2$ and t are presented.

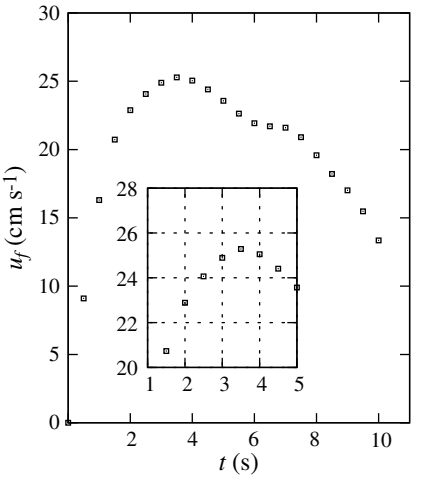

FIGURE 4. Experiment 01/29/13-5: front velocity history for the gravity current produced from a buoyancy source of $h_0/l_0 = 8$ cm/10 cm and $g'_0 = 167.10$ cm s^{-2}, i.e. $\epsilon \approx 0.17$, on a 9° slope. In this case the maximum front velocity $u_f \approx 25.28$ cm s^{-1} and occurs at $t \approx 3.5$ s.

4.1.2. *Quantitative results*

The fluid concentration images, e.g. figures 2 and 3, can be used to identify the front location as the foremost part of the gravity current. The front velocity can then be calculated as the time derivative of the front location history. Figure 4 shows the front velocity history for experiment 01/29/13-5. From the front velocity history, the acceleration and deceleration phases are clearly seen, with the maximum front velocity, $u_{f\,max} \approx 25.28$ cm s^{-1} reached at $t \approx 3.5$ s. From the relationship between $(x_f + x_0)^{3/2}$ and t in figure 5(a) for $\epsilon \approx 0.17$, it is observed that the power-law (2.10) applies in the early deceleration phase. Here, the departure of front location data from (2.10) towards the end of the deceleration phase is not a coincidence and was observed for all the relative density differences considered and for all the runs on $\theta = 9°$. From the relationship between $(x_f + x_0)^2$ and t in figure 5(b), it is observed that the power-law (2.13) applies towards the end of the deceleration phase, which confirms the notion that viscous effects could become more important in the late deceleration phase.

Figure 6 shows the relationships between $(x_f + x_0)^{3/2}$ and t and between $(x_f + x_0)^2$ and t for experiment 01/13/13-2 with $\epsilon \approx 0.05$ on $\theta = 9°$. The departure of front location data from the power-law (2.10) and approach to the power-law (2.13) in the late deceleration phase are again observed for $\epsilon \approx 0.05$. On comparing the flow patterns with the relationship between $(x_f + x_0)^{3/2}$ and t, we consistently found that the departure from power-law (2.10) is associated with the large-scale rolling-up of the moving heavy fluid and light ambient fluid. As an example, the flow pattern shown in figure 3 at $t = 9.5$ s occurs when the front location data deviate from the power-law (2.10), i.e. $t \gtrsim 8.0$ s in figure 5(a). These observations point to the fact that the front velocity may decay more rapidly when the front location data deviate from (2.10). The power-law (2.10) is obviously not applicable in the whole range of the deceleration phase. When the front location data deviate from (2.10), the head Reynolds numbers, $Re_H = u_f H/\nu$, were estimated in the range 2000–3000 for all the cases on $\theta = 9°$.

Where the power-law (2.10) applies, the early deceleration phase is best fitted by straight lines as shown in figure 5(a) and figure 6(a). The slope of the fitting

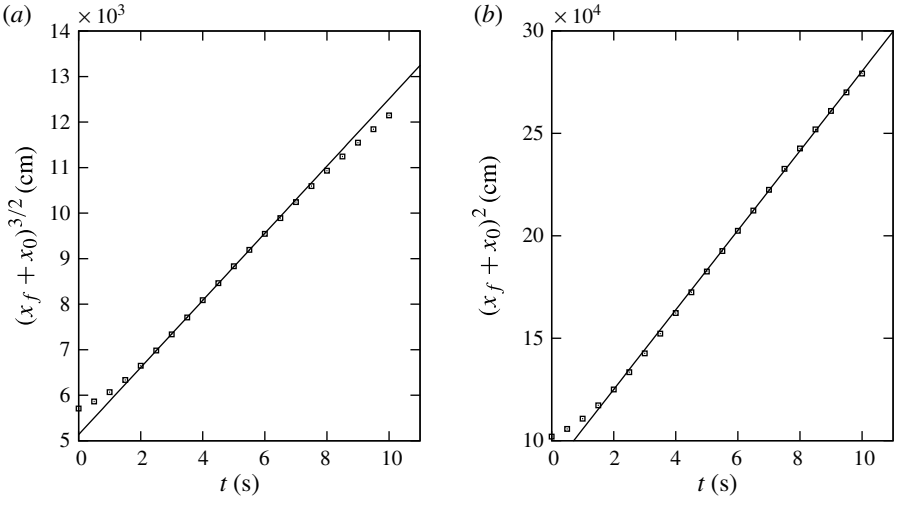

FIGURE 5. Experiment 01/29/13-5: relationship between (*a*) $(x_f + x_0)^{3/2}$ and t and (*b*) $(x_f + x_0)^2$ and t for the gravity current produced from a buoyancy source of $h_0/l_0 = 8$ cm/10 cm and $g_0' = 167.10\ \mathrm{cm\ s^{-2}}$, i.e. $\epsilon \approx 0.17$, on a 9° slope. The solid line in (*a*) represents the straight line of best fit to the early deceleration phase and the fitting equation is $(x_f + x_0)^{3/2} = 737.0(t + t_{I0})$, where $x_0 = 319.4$ cm and $t_{I0} = 7.0$ s. The solid line in (*b*) represents the straight line of best fit to the late deceleration phase and the fitting equation is $(x_f + x_0)^2 = 19410.4(t + t_{V0})$, where $t_{V0} = 4.4$ s. In this case the maximum front velocity $u_f \approx 25.28\ \mathrm{cm\ s^{-1}}$ and occurs at $t \approx 3.5$ s.

lines represents $K_M^{3/2} B_0'^{1/2}$ and the empirical constant K_M can be calculated. Table 3 lists the values of K_M in different cases. We note that for $\theta = 9°$, K_M increases from 2.97 to 3.48 as the relative density difference, ϵ, increases from 0.05 to 0.17. Based on our results, K_M is clearly not a universal constant. In the Boussinesq case reported by Maxworthy (2010), where $0.01 < \epsilon < 0.05$, K_M was observed to vary erratically between 2.5 and 2.9 for $\theta = 5.9°$ and 10.6°. Such observations are consistent with our expectations for K_M for low relative density differences. Where the power-law (2.13) applies, the late deceleration phase is best fitted by straight lines as shown in figure 5(*b*) and figure 6(*b*). The slope of the fitting lines then represents $K_V^2 B_0'^{2/3} A_0^{1/3} \nu^{-1/3}$ and the empirical constant K_V can be calculated, as also listed in table 3. Our results show that for $\theta = 9°$, K_V increases from 1.26 to 1.35 as the relative density difference increases from 0.05 to 0.17.

With the measured K_M and computed K_B, the amount of heavy fluid in the head region in the deceleration phase can be estimated theoretically via $\chi = (K_M/K_B)^3$. For example, for experiment 01/29/13-5 shown in figures 2–5, using $K_M^{3/2} B_0'^{1/2} = 737.0\ \mathrm{cm^{3/2}\ s^{-1}}$ and $B_0' = 13368.0\ \mathrm{cm^3\ s^{-2}}$, $K_M = 3.44$ is derived. With measured parameters $k \approx 0.25$ and $\alpha_0 = 0.0196$, $K_B = 5.26$ is then computed via (2.11) and therefore $\chi = 0.28$. As listed in table 3 and shown from figure 7, it is observed that the power-law (2.10) not only describes the front location data in the early deceleration phase but also provides a reasonable estimate for the amount of heavy fluid in the head region, even though the gravity current head may lose buoyancy as it propagates. Here the theoretical estimates for χ generally tend to fall below the maximum values of A_h/A_0 from experiments. It should be noted that the estimate

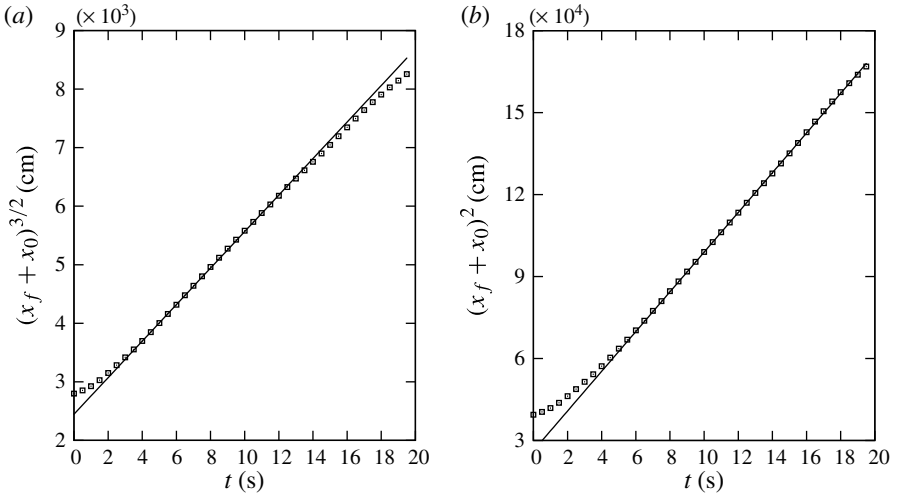

FIGURE 6. Experiment 01/13/13-2: relationship between (*a*) $(x_f + x_0)^{3/2}$ and t and (*b*) $(x_f + x_0)^2$ and t for the gravity current produced from a buoyancy source of $h_0/l_0 = 8$ cm/10 cm and $g_0' = 49.16$ cm s^{-2}, i.e. $\epsilon \approx 0.05$, on a 9° slope. The solid line in (*a*) represents the straight line of best fit to the early deceleration phase and the fitting equation is $(x_f + x_0)^{3/2} = 311.9(t + t_{I0})$, where $x_0 = 198.6$ cm, $t_{I0} = 7.8$ s. The solid line in (*b*) represents the straight line of best fit to the late deceleration phase and the fitting equation is $(x_f + x_0)^2 = 7267.4(t + t_{V0})$, where $t_{V0} = 3.6$ s. In this case the maximum front velocity $u_f \approx 13.09$ cm s^{-1} and occurs at $t \approx 6.5$ s.

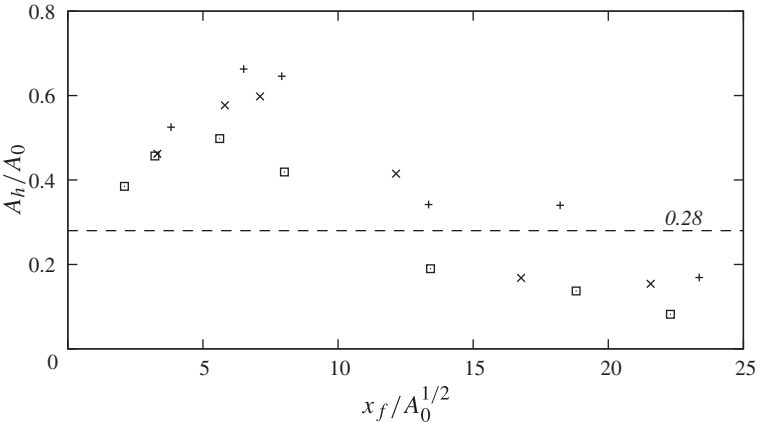

FIGURE 7. Ratio of the buoyancy in the head region to the total released buoyancy, A_h/A_0, against the front location normalized by $A_0^{1/2}$, where A_h/A_0 is evaluated using (3.1). Symbols: +, experiment 01/29/13-5 for $\epsilon \approx 0.17$ on $\theta = 9°$; ×, experiment 01/23/13-1 for $\epsilon \approx 0.17$ on $\theta = 6°$; ⊡, experiment 01/24/13-2 for $\epsilon \approx 0.17$ on $\theta = 2°$. Dashed line represents $\chi = 0.28$ which is estimated for $\theta = 9°$ via $\chi = (K_M/K_B)^3$ using measured parameters.

is based on the momentum principle and should be understood as a lower limit for the 'effective' or 'active' buoyancy that plays the role of driving mechanism. In the

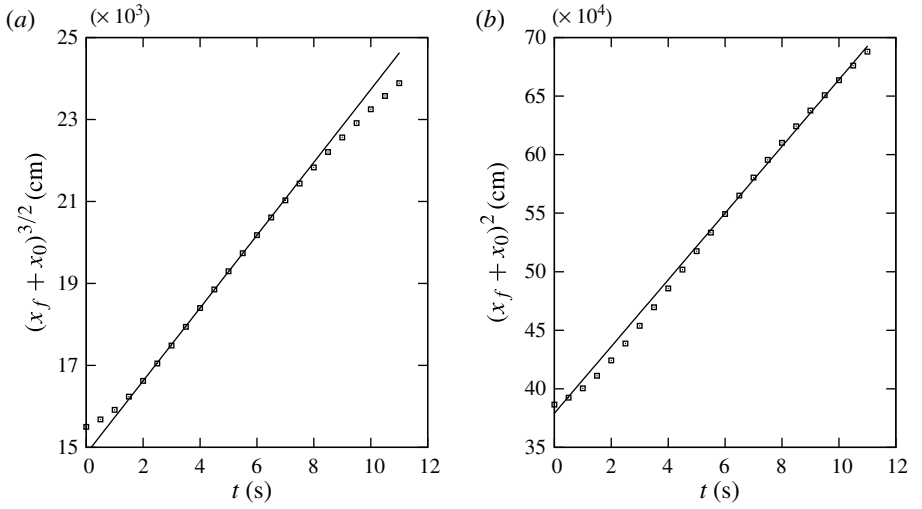

FIGURE 8. Experiment 01/23/13-1: relationship between (*a*) $(x_f + x_0)^{3/2}$ and t and (*b*) $(x_f + x_0)^2$ and t for the gravity current produced from a buoyancy source of $h_0/l_0 = 8\ \text{cm}/10\ \text{cm}$ and $g_0' = 166.73\ \text{cm s}^{-2}$, i.e. $\epsilon \approx 0.17$, on a 6° slope. The solid line in (*a*) represents the straight line of best fit to the early deceleration phase and the fitting equation is $(x_f + x_0)^{3/2} = 888.8(t + t_{I0})$, where $x_0 = 621.7$ cm and $t_{I0} = 16.7$ s. The solid line in (*b*) represents the straight line of best fit to the late deceleration phase and the fitting equation is $(x_f + x_0)^2 = 28491.8(t + t_{V0})$, where $t_{V0} = 13.3$ s. In this case the maximum front velocity $u_f \approx 23.28\ \text{cm s}^{-1}$ and occurs at $t \approx 3.5$ s.

head region, there may be more buoyancy-containing fluid as part of it is diluted or 'ineffective' in driving the gravitational convection.

4.2. *Gravity currents on $\theta = 6°$ slope*

The flow patterns of gravity currents on a 6° slope are qualitatively similar to those on a 9° slope in both the acceleration and deceleration phases. It is also observed that towards the end of the deceleration phase, large-scale rolling-up of the moving heavy fluid and light ambient fluid occurs on a 6° slope as reported previously for the 9° slope.

Figure 8 shows $(x_f + x_0)^{3/2}$ versus t and $(x_f + x_0)^2$ versus t for gravity currents on a 6° slope with $\epsilon \approx 0.17$. As for $\theta = 9°$, the power-law (2.10) applies in the early deceleration phase here for $\theta = 6°$. Towards the end of the deceleration phase, the front location data deviate from the power-law (2.10) and approach the power-law (2.13) as the large-scale rolling-up of the two fluids occurs. When the front location data deviate from (2.10), the head Reynolds numbers were estimated in the range 2000–3000 for all cases with $\theta = 6°$.

As reported previously, it is observed that K_M increases with ϵ, and the numerical values of K_M at $\theta = 6°$ are consistently greater than those at $\theta = 9°$. In the Boussinesq case for $\theta = 5.9°$ and 10.6° considered by Maxworthy (2010), K_M appeared to vary erratically between 2.5 and 2.9 without strong dependence on θ. From table 3 and figure 14, we show that as the relative density difference increases, K_M assumes a maximum value at $\theta \approx 6°$. Our results also indicate that K_V increases with ϵ and K_V reaches a maximum value at $\theta \approx 6°$, as shown in figure 15.

Case	K_M	K_B	K_V	χ
9I	$3.48^{+0.06}_{-0.04}$	$5.48^{+0.15}_{-0.23}$	$1.35^{+0.01}_{-0.02}$	$0.26^{+0.02}_{-0.02}$
9II	$3.28^{+0.07}_{-0.05}$	$4.81^{+0.14}_{-0.26}$	$1.29^{+0.02}_{-0.03}$	$0.32^{+0.05}_{-0.04}$
9III	$2.97^{+0.04}_{-0.06}$	$4.38^{+0.05}_{-0.03}$	$1.26^{+0.03}_{-0.04}$	$0.31^{+0.02}_{-0.01}$
6I	$3.96^{+0.07}_{-0.07}$	$7.21^{+0.06}_{-0.07}$	$1.64^{+0.02}_{-0.03}$	$0.17^{+0.01}_{-0.01}$
6II	$3.36^{+0.04}_{-0.03}$	$4.90^{+0.15}_{-0.29}$	$1.42^{+0.01}_{-0.02}$	$0.33^{+0.07}_{-0.04}$
6III	$3.22^{+0.05}_{-0.05}$	$4.37^{+0.09}_{-0.12}$	$1.38^{+0.03}_{-0.02}$	$0.40^{+0.03}_{-0.03}$
2I	$3.93^{+0.06}_{-0.04}$	$7.20^{+0.61}_{-0.65}$	$1.64^{+0.04}_{-0.03}$	$0.17^{+0.04}_{-0.03}$
2II	$3.10^{+0.02}_{-0.03}$	$4.71^{+0.41}_{-0.24}$	$1.33^{+0.08}_{-0.06}$	$0.29^{+0.05}_{-0.06}$
2III	$2.95^{+0.06}_{-0.03}$	$4.18^{+0.06}_{-0.05}$	$1.30^{+0.01}_{-0.01}$	$0.35^{+0.04}_{-0.01}$
0I	$1.57^{+0.03}_{-0.05}$	—	—	—
0II	$1.56^{+0.03}_{-0.04}$	—	—	—
0III	$1.61^{+0.04}_{-0.03}$	—	—	—

TABLE 3. Table showing experimental constants and the estimated effective buoyancy ratio, χ, in the deceleration phase. Each value is the average of five experiments. The lock geometry, i.e. $h_0/l_0 = 8$ cm/10 cm, is maintained fixed for all experiments. The error estimates are to add and subtract the maximum and minimum values and are not the r.m.s. estimates.

The amount of heavy fluid in the head region can be estimated via $\chi = (K_M/K_B)^3$, as listed in table 3. We note that the theoretical estimates for χ are consistent with A_h/A_0 derived from the concentration images, as shown in figure 7, but the theoretical estimates tend to fall below the maximum values of A_h/A_0. Based on our results for A_h/A_0, approximately 60 % or more of the heavy fluid in the lock is discharged into the head at most, as listed in table 1.

4.3. *Gravity currents on $\theta = 2°$ slope*

For gravity currents on a 2° slope, we first note that the maximum front velocity occurs at a earlier time and a shorter distance from the gate than those for $\theta = 6°$ and 9°. The mixing at $\theta = 2°$ is obviously less intense than $\theta = 6°, 9°$ and the roller behind the head no longer exists at the end of the acceleration phase, as shown in figure 9 at $t = 2.5$ s.

The gravity current head on $\theta = 2°$ still has a 'cloud' shape, which appears to be more streamlined compared with those on $\theta = 6°$ and 9° and the large-scale rolling-up of the heavy fluid and light ambient fluid towards the end of the deceleration phase does not exist here.

Figure 10 shows the relationships between $(x_f + x_0)^{3/2}$ and t and between $(x_f + x_0)^2$ and t for gravity currents on a 2° slope with $\epsilon \approx 0.17$. While the approach to the power-law (2.10) is from above for $\theta = 6°$ and 9°, it is from below in $\theta = 2°$ due to the low slope angle. As in previous cases, (2.10) applies only in the early deceleration phase and the power-law (2.13) applies in the late deceleration phase. The deviation from (2.10) appears when the gravity current propagates sufficiently far into the deceleration phase with the head Reynolds numbers estimated in the range 2000–3000. What differs from the observations for $\theta = 6°$ and 9° is that the gravity

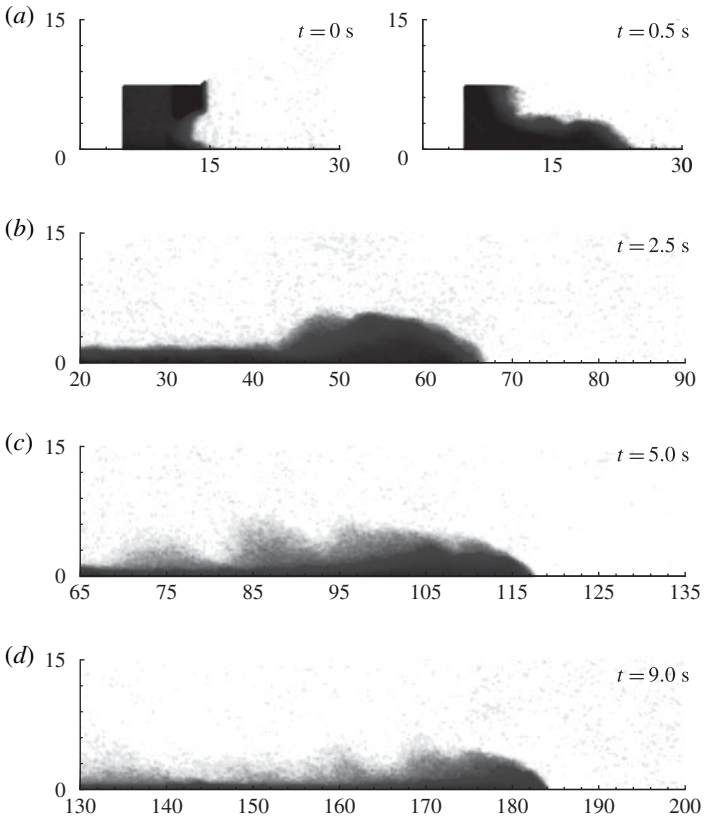

FIGURE 9. Experiment 01/24/13-2: fluid concentration images for a gravity current from a buoyancy source of $h_0/l_0 = 8$ cm/10 cm and $g_0' = 167.01$ cm s^{-2} propagating on a 2° slope. Distances in the downslope and wall-normal directions are in units of centimetres. Time instants are chosen at $t = 0$, 0.5, 2.5, 5.0 and 9.0 s. In this case the maximum front velocity $u_f \approx 21.64$ cm s^{-1} and occurs at $t \approx 2.5$ s.

current head maintains a streamlined shape without large-scale mixing towards the end of the deceleration phase.

As listed in table 3 and shown in figures 14 and 15 below, both K_M and K_V increase with ϵ and their values at $\theta = 2°$ become slightly lower than at $\theta = 6°$. The theoretical estimates for the heavy fluid in the head, χ, show agreement with A_h/A_0. Based on our results for $\theta = 2°$, the maximum buoyancy in the head is approximately 50 % or more of the heavy fluid originally contained in the lock. As listed in table 1, the maximum values of the fraction of heavy fluid in the head, i.e. $A_{h,max}/A_0$, for $\theta = 2°$ tend to be slightly lower than those for $\theta = 6°$ and 9°.

4.4. *Gravity currents on $\theta = 0°$ slope*

Concentration images for the gravity current on a horizontal boundary are shown in figure 11. In the experiments for $\theta = 0°$, the lock was submerged beneath the surface by approximately 40 cm, and the lock height to ambient depth ratio is below 0.2, which is also termed partial-depth lock-exchange flow (Marino *et al.* 2005).

From the concentration images, the initiation process of a gravity current is similar to those on $\theta = 9°$, 6° but the mixing with ambient fluid is not as violent. Specifically,

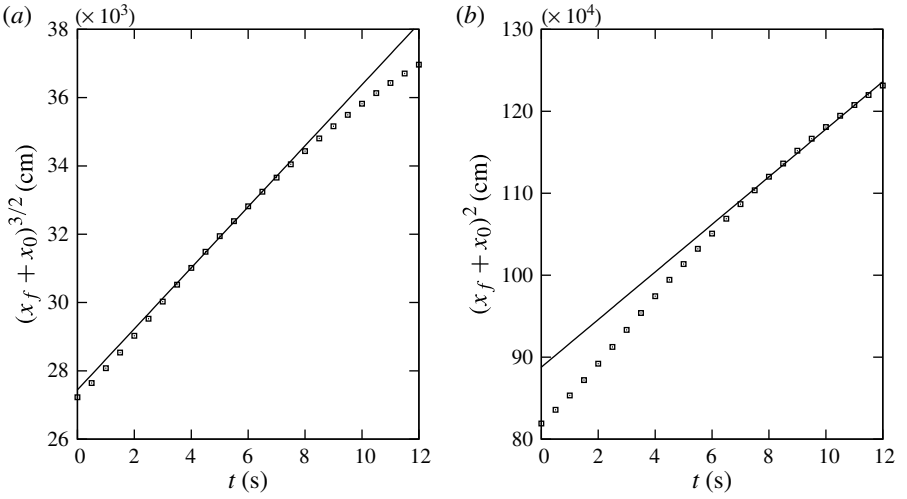

FIGURE 10. Experiment 01/24/13-2: relationship between (*a*) $(x_f + x_0)^{3/2}$ and t and (*b*) $(x_f + x_0)^2$ and t for the gravity current produced from a buoyancy source of $h_0/l_0 = 8$ cm/10 cm and $g_0' = 167.01$ cm s^{-2}, i.e. $\epsilon \approx 0.17$, on a 2° slope. The solid line in (*a*) represents the straight line of best fit to the early deceleration phase and the fitting equation is $(x_f + x_0)^{3/2} = 893.4(t + t_{I0})$, where $x_0 = 905.5$ cm, $t_{I0} = 30.7$ s. The solid line in (*b*) represents the straight line of best fit to the late deceleration phase and the fitting equation is $(x_f + x_0)^2 = 29026.6(t + t_{V0})$, where $t_{V0} = 30.6$ s. In this case the maximum front velocity $u_f \approx 21.64$ cm s^{-1} and occurs at $t \approx 2.5$ s.

a roller behind the head at the end of the acceleration phase was not present for $\theta = 0°$, neither was it for $\theta = 2°$. The head and tail currents seemed to join up in both the acceleration and deceleration phases.

It is already known for lock-exchange flows that in the inertial phase, the front location follows the asymptote $\tilde{x}_f \sim \tilde{t}^{2/3}$ while in the viscous phase, $\tilde{x}_f \sim \tilde{t}^{3/8}$ and $\tilde{x}_f \sim \tilde{t}^{1/5}$ were reported by Hoult (1972) and Huppert (1982), respectively. Here the front location is normalized by l_0 and the time is normalized by a characteristic time scale, $l_0/\sqrt{g_0' h_0}$.

As shown in figure 12, the inertial phase and a transition to the viscous phase are both identifiable for gravity currents on $\theta = 0°$ with $\epsilon \approx 0.05$, 0.10 and 0.17. The coefficient of proportionality between $\tilde{x}_f$ and $\tilde{t}^{2/3}$ is K_M, as indicated in (2.14). Interestingly, the inertial phase exists for all three density differences $\epsilon \approx 0.05$, 0.10 and 0.17 when $20 \lesssim \tilde{t} \lesssim 40$. When $\tilde{t} \gtrsim 40$, deviation from the inertial phase indicates a transition to the viscous phase, as shown by the approach of the front location data to the dash-dotted lines in figure 12(*b*). The head Reynolds numbers for the cases on $\theta = 0°$ were in the range 1000–2000 when a transition to the viscous phase was observed.

For gravity currents on $\theta = 0°$, the head height does not increase or even decreases slowly during the motion. As such, extrapolation of head height in the upslope direction to identify the virtual origin becomes unfeasible and the front location data could be recast in the power-law form by stipulating $x_0 = 0$ (Beghin *et al.* 1981), i.e. that the front location is now measured from the lock gate.

Figure 13 shows ${x_f}^{3/2}$ versus t for gravity currents on $\theta = 0°$ with $\epsilon \approx 0.17$(*a*) and 0.05(*b*). It is observed that (2.14) applies in the inertial phase. Deviation from (2.14)

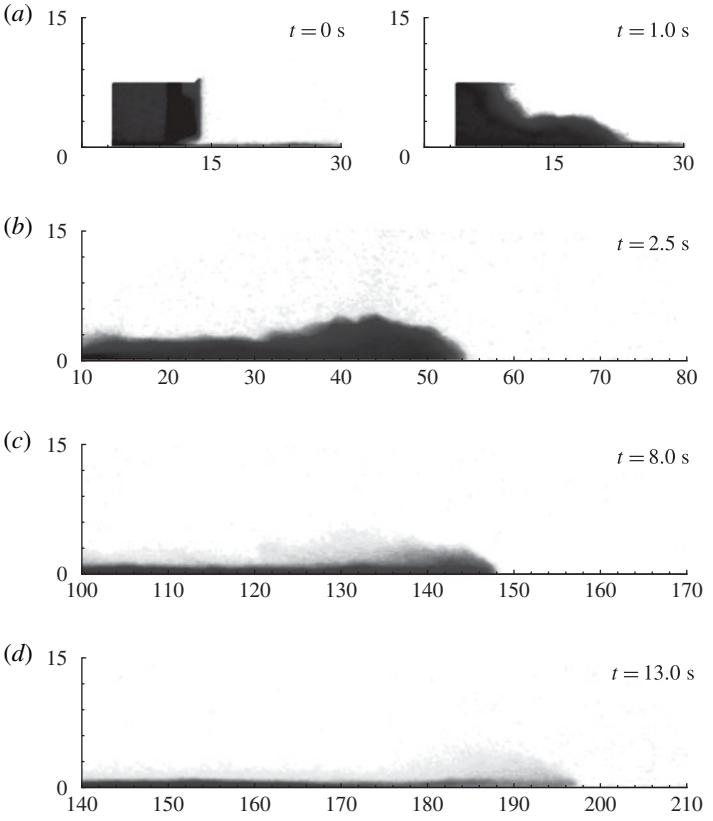

FIGURE 11. Experiment 02/05/13-2: fluid concentration images for the gravity current from a buoyancy source of $h_0/l_0 = 8$ cm/10 cm and $g'_0 = 167.55$ cm s^{-2} propagating on a 0° slope. Distances in the downslope and wall-normal directions are in units of centimetres. Time instants are chosen at $t = 0$, 1.0, 2.5, 8.0 and 13.0 s. In this case the maximum front velocity $u_f \approx 19.55$ cm s^{-1} and occurs at $t \approx 2.5$ s.

appears again in the transition to the viscous phase. It should be pointed out that when the deviation from (2.14) occurs, the large-scale mixing identified on $\theta = 9°$, 6° is not present on $\theta = 0°$. The gravity current maintains a more streamlined head in the deceleration phase as on $\theta = 2°$.

Mindful that the thermal theory was specifically developed for gravity currents down an inclined boundary, $\theta = 0°$ results in $K_B = 0$ and to theoretically estimate the parameter $\chi = (K_M/K_B)^3$ seems inappropriate. However, we may still estimate K_M using (2.14) in the inertial phase.

As listed in table 3, K_M varies in the range between 1.56 and 1.61 for $\theta = 0°$ with $\epsilon = 0.17$, 0.10 and 0.05. From our results, no strong dependence of K_M on ϵ can be inferred on $\theta = 0°$. On the other hand, our results show excellent agreement with previous reports for the Boussinesq gravity currents on a horizontal boundary. Among others, $K_M = 1.6$ and 1.47 have been reported by Hoult (1972) and Huppert & Simpson (1980), respectively, while more recently, Marino *et al.* (2005) suggested $1.4 \lesssim K_M \lesssim 1.8$ for partial-depth lock-exchange flows.

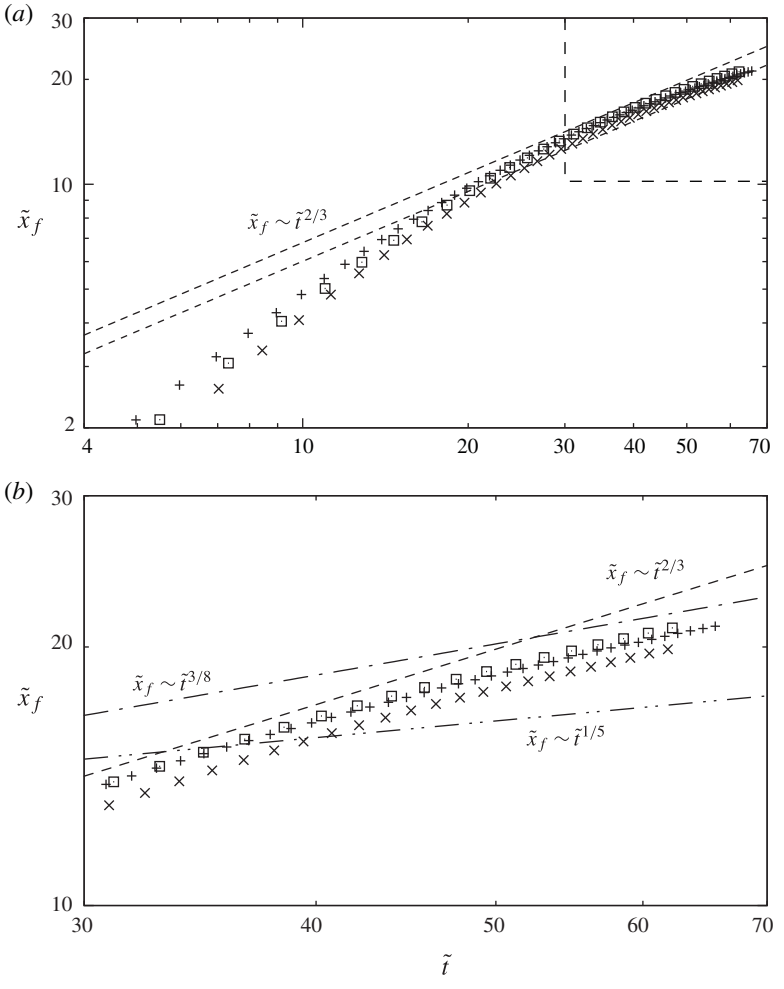

FIGURE 12. The front location, $\tilde{x}_f$, versus time, $\tilde{t}$, on a log–log scale for experiment 02/05/13-2 with $g_0' = 167.55$ cm s^{-2}, i.e. $\epsilon \approx 0.17$ (□), experiment 02/05/13-3 with $g_0' = 98.92$ cm s^{-2}, i.e. $\epsilon \approx 0.10$ (×), and experiment 02/04/13-2 with $g_0' = 49.45$ cm s^{-2}, i.e. $\epsilon \approx 0.05$ (+) on $\theta = 0°$. In all cases, the gravity currents are produced from a buoyancy source of $h_0/l_0 = 8$ cm/10 cm. The front location is non-dimensionalized by l_0 and time is non-dimensionalized by $l_0/\sqrt{g_0' h_0}$. The dashed lines in (*a*) represent the asymptotes for the inertial phase: $\tilde{x}_f \sim \tilde{t}^{2/3}$. (*b*) Close-up view for $30 \leqslant \tilde{t} \leqslant 70$, where the dashed line indicates $\tilde{x}_f \sim \tilde{t}^{2/3}$, and the dashed-dotted lines represent the asymptotes for the viscous phase, i.e. $\tilde{x}_f \sim \tilde{t}^{3/8}$ by Hoult (1972) and $\tilde{x}_f \sim \tilde{t}^{1/5}$ by Huppert (1982).

5. Conclusions

Gravity currents produced from an instantaneous buoyancy source propagating on an inclined boundary as the relative density difference varies in the range of $0.05 \leqslant \epsilon \leqslant 0.17$ and the slope angle varies in the range of $0° \leqslant \theta \leqslant 9°$ are presented.

First, we consider the applicability of power-law (2.10) for the front location history in the deceleration phase. This relationship was reported by Maxworthy (2010) to be robust in the whole range of the deceleration phase for the Boussinesq case. As we found by performing the experiments on different slopes and with different relative

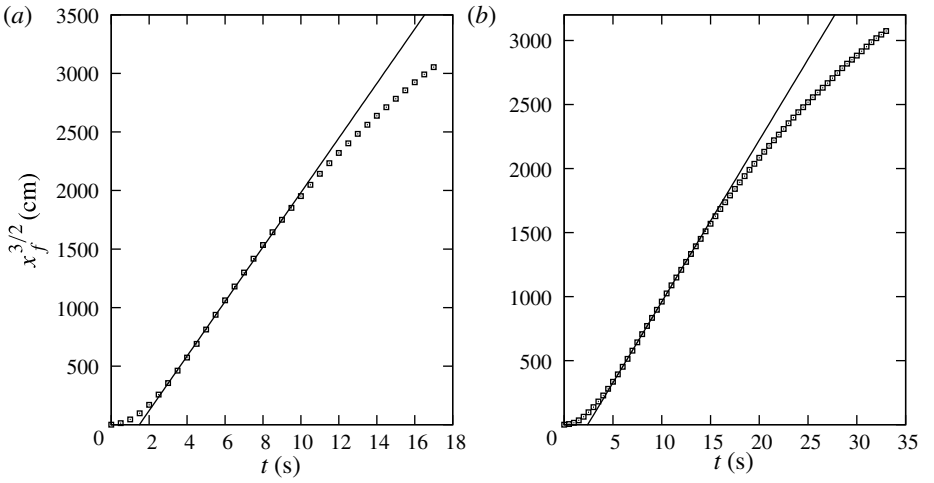

FIGURE 13. Relationships between $x_f^{3/2}$ and t for (a) experiment 02/05/13-2 with $g_0' = 167.55$ cm s^{-2}, i.e. $\epsilon \approx 0.17$, and (b) experiment 02/04/13-2 with $g_0' = 49.45$ cm s^{-2}, i.e. $\epsilon \approx 0.05$, on a horizontal boundary. The front location is measured from the gate. The solid lines represent the straight lines of best fit to the inertial phase. The fitting equation for (a) is $x_f^{3/2} = 232.8(t - t_{I0})$, where $t_{I0} = 1.5$ s and in this case the maximum front velocity $u_f \approx 19.55$ cm s^{-1} and occurs at $t \approx 2.5$ s. The fitting equation for (b) is $x_f^{3/2} = 126.3(t - t_{I0})$, where $t_{I0} = 2.4$ s and in this case the maximum front velocity $u_f \approx 10.92$ cm s^{-1} and occurs at $t \approx 4.5$ s.

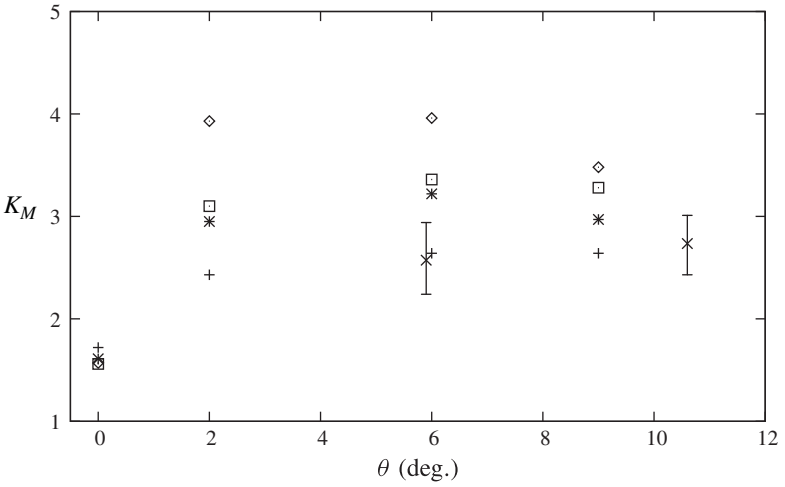

FIGURE 14. Experimental constant K_M versus slope angle θ at different relative density differences: $\diamond$, $\epsilon \approx 0.17$; $\boxdot$, $\epsilon \approx 0.10$; $*$, $\epsilon \approx 0.05$; $+$, experimental data for $\epsilon \approx 0.02$ reported in Dai (2013);$\times$, experimental data for $0.01 < \epsilon < 0.05$ reported in Maxworthy (2010).

density differences, the power-law (2.10) applies only in the early deceleration phase for both the Boussinesq and non-Boussinesq cases. In the late deceleration phase, viscous effects could become more important and the front location data deviate from

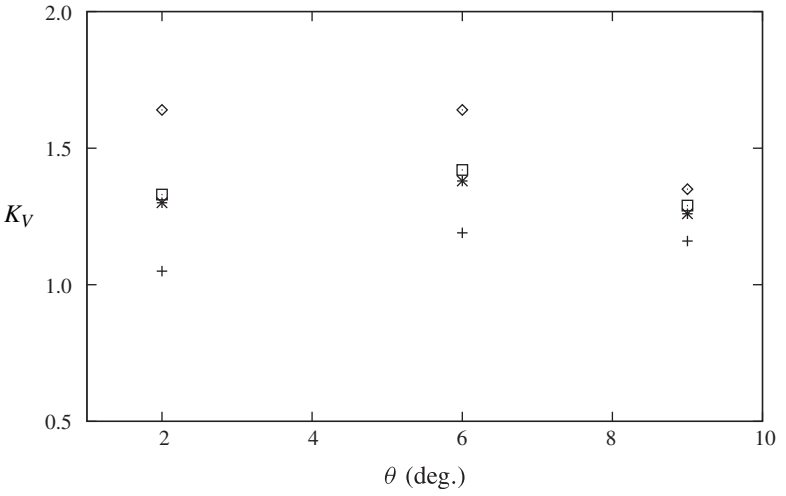

FIGURE 15. Experimental constant K_V versus slope angle θ at different relative density differences: $\diamond$, $\epsilon \approx 0.17$; $\boxdot$, $\epsilon \approx 0.10$; $*$, $\epsilon \approx 0.05$; $+$, experimental data for $\epsilon \approx 0.02$ derived from Dai (2013).

(2.10) and approach the power-law (2.13). It is interesting to note that for gravity currents on $\theta = 6°, 9°$, large-scale mixing between the heavy and light ambient fluids occurs in the late deceleration phase; for gravity currents on $\theta = 0°, 2°$, the head maintains a more streamlined shape without violent mixing when the deviation from the power-law (2.10) is observed. Our findings indicate that depending on the slope angle, the flow patterns in the late deceleration phase of a gravity current may be qualitatively different.

Secondly, in the Boussinesq case considered by Maxworthy (2010), K_M was reported to vary erratically in the range approximately between 2.5 and 2.9 when $0.01 < \epsilon < 0.05$ at $\theta = 5.9°$ and $10.6°$ without strong dependence on the slope angle. Our results do not support K_M to be a universal constant. We showed that for sufficiently large slope angle, $\theta \gtrsim 2°$, K_M increases as the relative density difference increases and K_M assumes its maximum value at $\theta \approx 6°$. For sufficiently low relative density differences, namely the Boussinesq case, the values of K_M reported by Maxworthy (2010) are in accordance with our expectations. In addition, when the front location data deviate from (2.10) and approach (2.13), our results also indicate that K_V increases with the relative density difference and assumes a maximum value at $\theta \approx 6°$.

Using the power-law (2.10), it is possible to estimate the fraction of heavy fluid in the lock that is contained in the head, via $\chi = (K_M/K_B)^3$. We showed that (2.10) applies in the early deceleration phase for both the Boussinesq and non-Boussinesq cases. The theoretical estimates are in good agreement with the experimental results, although the theoretical estimates tend to be lower than the maximum values of the fraction derived from experimental data. We need to point out that (2.10) is essentially based on the momentum principle and the theoretical estimate for χ should be understood as a lower bound for the 'effective' or 'active' buoyancy in driving the gravitational convection.

For gravity currents on sufficiently low slope angles, i.e. $\theta \approx 0°$, it is well understood that the inertial phase is followed by the viscous phase where viscous

effects become more important. It is then not irrational to infer that viscous effects could be unexpectedly more important when the front location data deviate from the power-law (2.10). Indeed, our findings support the notion that viscous effects could become more important in the late deceleration phase, which appears to be an exception to the general belief that viscous effects are unimportant at Reynolds numbers above 1000.

One of the limitations in this study is the range of slope angle investigated due to the limited depth of our channel, as has been the case in many previously published works. The aim of investigating the influence of density difference on the propagation of gravity currents is achieved in a somewhat limited range of density ratio, i.e. $0.85 \leqslant \gamma \leqslant 0.95$, or equivalently in terms of the relative density difference, i.e. $0.05 \leqslant \epsilon \leqslant 0.17$, due to the solubility of sodium chloride in water at room temperature. For higher density differences, it has been documented that the density ratio can reach as low as 0.61 (Lowe *et al.* 2005) with the help of sodium iodide, which is an expensive material typically used for radiation detection and other medical purposes. It is hoped that further studies on gravity currents on higher slope angles and with even higher relative density differences will be conducted when the apparatus and working fluids are available.

Acknowledgements

The author wishes to thank Ben Maurer, Paul Linden, and Stuart Dalziel at the University of Cambridge, S. Balachandar at the University of Florida, Marcelo Garcia and Gary Parker at the University of Illinois at Urbana-Champaign for encouragement at different stages of the work. The author also thanks Mr H. Y. Chou for the help in running the experiments. Funding support from the National Science Council of Taiwan through grants NSC-98-2218-E-032-007 and NSC-101-2628-E032-003-MY3 is greatly acknowledged. The author wishes to dedicate this work to the memory of Professor Tony Maxworthy at the University of Southern California, who recently passed away but will remain a role model for those who carry on.

REFERENCES

ADDUCE, C., SCIORTINO, G. & PROIETTI, S. 2012 Gravity currents produced by lock-exchanges: experiments and simulations with a two layer shallow-water model with entrainment. *J. Hydraul. Engng* **138** (2), 111–121.

ALLEN, J. 1985 *Principles of Physical Sedimentology*. Allen & Unwin.

BAINES, P. G. 2001 Mixing in flows down gentle slopes into stratified environments. *J. Fluid Mech.* **443**, 237–270.

BAINES, P. G. 2005 Mixing regimes for the flow of dense fluid down slopes into stratified environments. *J. Fluid Mech.* **538**, 245–267.

BATCHELOR, G. K. 1967 *An Introduction to Fluid Dynamics*. Cambridge University Press.

BEGHIN, P., HOPFINGER, E. J. & BRITTER, R. E. 1981 Gravitational convection from instantaneous sources on inclined boundaries. *J. Fluid Mech.* **107**, 407–422.

BIRMAN, V. K., BATTANDIER, B. A., MEIBURG, E. & LINDEN, P. F. 2007 Lock-exchange flows in sloping channels. *J. Fluid Mech.* **577**, 53–77.

BIRMAN, V. K., MARTIN, J. E. & MEIBURG, E. 2005 The non-Boussinesq lock-exchange problem. Part 2. High-resolution simulations. *J. Fluid Mech.* **537**, 125–144.

BRITTER, R. E. & LINDEN, P. F. 1980 The motion of the front of a gravity current travelling down an incline. *J. Fluid Mech.* **99**, 531–543.

CANTERO, M., LEE, J., BALACHANDAR, S. & GARCIA, M. 2007 On the front velocity of gravity currents. *J. Fluid Mech.* **586**, 1–39.

CENEDESE, C. & ADDUCE, C. 2008 Mixing in a density driven current flowing down a slope in a rotating fluid. *J. Fluid Mech.* **604**, 369–388.

DADE, W. B., LISTER, J. R. & HUPPERT, H. E. 1994 Fine-sediment deposition from gravity surges on uniform slopes. *J. Sed. Res.* **64**, 423–432.

DAI, A. 2013 Experiments on gravity currents propagating on different bottom slopes. *J. Fluid Mech.* **731**, 117–141.

DAI, A. & GARCIA, M. 2010 Gravity currents down a slope in deceleration phase. *Dyn. Atmos. Oceans* **49**, 75–82.

DALZIEL, S. B. 2012 *DigiFlow User Guide*. Dalziel Research Partners.

ELLISON, T. H. & TURNER, J. S. 1959 Turbulent entrainment in stratified flows. *J. Fluid Mech.* **6**, 423–448.

FANNELOP, T. K. 1994 *Fluid Mechanics for Industrial Safety and Environmental Protection*. Elsevier.

GROBELBAUER, H. P., FANNELOP, T. K. & BRITTER, R. E. 1993 The propagation of intrusion fronts of high density ratios. *J. Fluid Mech.* **250**, 669–687.

HOPFINGER, E. J. 1983 Snow avalanche motion and related phenomena. *Annu. Rev. Fluid Mech.* **15**, 47–76.

HOULT, D. P. 1972 Oil spreading on the sea. *Annu. Rev. Fluid Mech.* **4**, 341–368.

HUPPERT, H. 1982 The propagation of two-dimensional and axisymmetric viscous gravity currents over a rigid horizontal boundary surface. *J. Fluid Mech.* **121**, 43–58.

HUPPERT, H. & SIMPSON, J. 1980 The slumping of gravity currents. *J. Fluid Mech.* **99**, 785–799.

KELLER, J. J. & CHYOU, Y. P. 1991 On the hydraulic lock exchange problem. *J. Appl. Math. Phys.* **42**, 874–909.

LA ROCCA, M., ADDUCE, C., LOMBARDI, V., SCIORTINO, G. & HINKERMANN, R. 2012*a* Developement of a lattice Boltzmann method for two-layered shallow-water flow. *Intl J. Numer. Meth. Fluids* **70** (8), 1048–1072.

LA ROCCA, M., ADDUCE, C., SCIORTINO, G., BATEMAN, P. A. & BONIFORTI, M. A. 2012*b* A two-layer shallow water model for 3d gravity currents. *J. Hydraul. Res.* **50** (2), 208–217.

LA ROCCA, M., ADDUCE, C., SCIORTINO, G. & PINZON, A. B. 2008 Experimental and numerical simulation of three-dimensional gravity currents on smooth and rough bottom. *Phys. Fluids* **20** (10), 106603.

LOWE, R. J., ROTTMAN, J. W. & LINDEN, P. F. 2005 The non-Boussinesq lock-exchange problem. Part 1. Theory and experiments. *J. Fluid Mech.* **537**, 101–124.

MARINO, B., THOMAS, L. & LINDEN, P. 2005 The front condition for gravity currents. *J. Fluid Mech.* **536**, 49–78.

MAXWORTHY, T. 2010 Experiments on gravity currents propagating down slopes. Part 2. The evolution of a fixed volume of fluid released from closed locks into a long, open channel. *J. Fluid Mech.* **647**, 27–51.

MAXWORTHY, T. & NOKES, R. I. 2007 Experiments on gravity currents propagating down slopes. Part 1. The release of a fixed volume of heavy fluid from an enclosed lock into an open channel. *J. Fluid Mech.* **584**, 433–453.

MONAGHAN, J. J., CAS, R. A. F., KOS, A. M. & HALLWORTH, M. 1999 Gravity currents descending a ramp in a stratified tank. *J. Fluid Mech.* **379**, 39–69.

NOGUEIRA, H. I. S., ADDUCE, C., ALVES, E. & FRANCA, M. J. 2013*a* Analysis of lock-exchange gravity currents over smooth and rough beds. *J. Hydraul Res.* **51** (4), 417–431.

NOGUEIRA, H. I. S., ADDUCE, C., ALVES, E. & FRANCA, M. J. 2013*b* Image analysis technique applied to lock-exchange gravity currents. *Meas. Sci. Technol.* **24**, 047001.

RASTELLO, M. & HOPFINGER, E. J. 2004 Sediment-entraining suspension clouds: a model of powder-snow avalanches. *J. Fluid Mech.* **509**, 181–206.

ROSS, A. N., DALZIEL, S. B. & LINDEN, P. F. 2006 Axisymmetric gravity currents on a cone. *J. Fluid Mech.* **565**, 227–253.

SEON, T., ZNAIEN, J., PERRIN, B., HINCH, E. J., SALIN, D. & HULIN, J. P. 2007 Front dynamics and macroscopic diffusion in buoyant mixing in tilted tubes. *Phys. Fluids* **19**, 125105.

SHIN, J., DALZIEL, S. & LINDEN, P. 2004 Gravity currents produced by lock exchange. *J. Fluid Mech.* **521**, 1–34.

SIMPSON, J. 1997 *Gravity Currents,* 2nd edn. Cambridge University Press.